CHAPTER 3

Results and discussion

3.1 Static calculations

3.1.1 Geometry optimizations

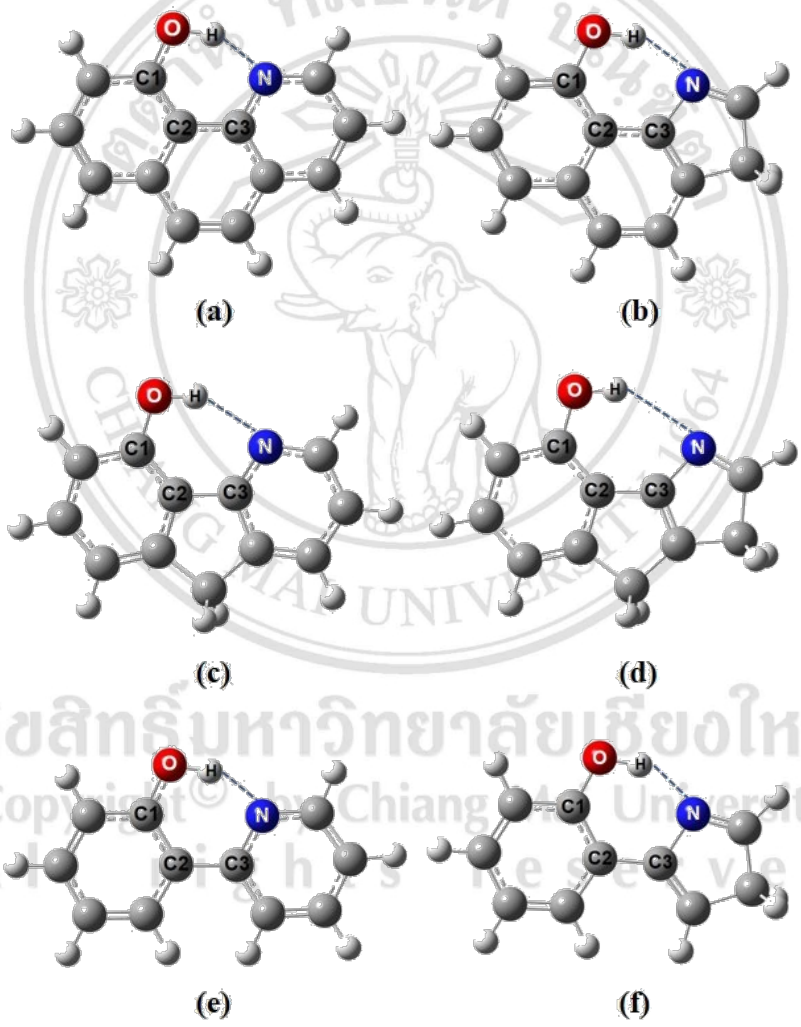

Figure 3.1 Optimized geometries of HBQ and its derivatives computed at B3LYP/TZVP level: (a) HBQ, (b) HBID, (c) IPDO, (d) IPRO, (e) PDP, and (f) PRP. Intramolecular hydrogen-bonded distances show in dashed line and the atoms involving proton transfer were labeled

Geometries of HBQ and its derivatives based on the DFT and TD-DFT methods for the S_0 and S_1 states. The optimized normal form and tautomer form of HBQ and its derivatives were obtained at B3LYP/TZVP basis set level in the gas phase to study the effect of geometry changes of HBQ and its derivatives. Figure 3.1 shows ground state optimized geometries of HBQ and its derivatives; (1a) HBQ, (1b) HBID, (1c) IPDO, (1d) IPRO, (1e) PDP, and (1f) PRP, where the relevant proton transfer and dihedral angle atoms are numbered. The optimized geometry parameters of normal form such as hydrogen bond distances (O−H), intramolecular hydrogen-bonded distances (N···H), the important distances between heavy atoms (O···N, and C1···N), and a dihedral angle of HBQ and its derivatives at S_0 and S_1 states are listed in Table 1. From Table 3.1, all compounds have a planar structure. The calculated lengths of O−H bond in the S_0 state for HBQ, HBID, IPDO, IPRO, PDP, and PRP are 0.995, 0.980, 0.978, 0.969, 0.997, and 0.986 Å, respectively. In the S_1 state, these distances are 0.995, 0.980, 0.978, 0.969, 0.997, and 0.986 Å, respectively. The O−H bond lengths are not different in the S_1 state for all compounds. Meanwhile, the N···H distances of HBQ, HBID, IPDO, IPRO, PDP, and PRP are 1.706, 1.878, 2.075, 2.445, 1.675 and 1.759 Å in S_0 state, respectively, but they drastically reduce to be 1.594, 1.712, 1.838, 2.131, 1.504, and 1.518 Å in the S_1 state, respectively. The N···H bond lengths are shortened in the S_1 state of all compounds. Moreover, the O···N distances connecting the intramolecular hydrogen bond in S_0 state of HBQ, HBID, IPDO, IPRO, PDP, and PRP are 2.605, 2.753, 2.926, 3.263, 2.578, and 2.918 Å, respectively. Upon photoexcitation, these distances change to 2.513, 2.607, 2.730, 2.989, 2.457, and 2.439 Å, respectively. The O···N bond lengths are shortened in the S_1 state of all compounds. Similarly, the C1···N distances in S_0 state of HBQ, HBID, IPDO, IPRO, PDP, and PRP are 2.868, 3.020, 3.094, 3.355, 2.840, and 2.918 Å, respectively. The C1···N distance of all compounds are shortened in the S_1 state compared with the S_0 state (2.822, 2.924, 2.999, 3.198, 2.761, and 2.809 Å). The shortened distances of N···H, O···N, and C1···N indicate that the intramolecular hydrogen bonds are strengthened in the S_1 state.

Table 3.1 Summary of hydrogen bond distances (O−H), intramolecular hydrogen-bonded distances (N···H), the important distances between heavy atoms (O···N, and C1···N) (Å), and a dihedral angle (°) of HBQ and its derivatives (normal form) computed at B3LYP/TZVP level

Compound	State	Distance (Å)				Dihedral angle (°)
		O−H	N···H	O···N	C1···N	C1C2C3N
HBQ	S_0	0.995	1.706	2.605	2.868	0
	S_1	0.995	1.594	2.513	2.822	0
HBID	S_0	0.980	1.878	2.753	3.020	0
	S_1	0.980	1.712	2.607	2.924	0
IPDO	S_0	0.978	2.075	2.926	3.094	0
	S_1	0.978	1.838	2.730	2.999	0
IPRO	S_0	0.969	2.445	3.263	3.355	0
	S_1	0.969	2.131	2.989	3.198	0
PRP	S_0	0.997	1.675	2.578	2.840	0
	S_1	0.997	1.504	2.439	2.761	0
PDP	S_0	0.986	1.759	2.643	2.918	0
	S_1	0.986	1.518	2.439	2.809	0

In addition, an effective rule for evidence of excited-state hydrogen bond strengthening or weakening through an electronic spectral bathochromic shift or hypsochromic shift induced by the intramolecular hydrogen bonding interactions have been proposed by Han and co-worker [69, 70]. The calculated IR spectra of all compound in the vibrational regions of the O−H stretching mode related with PT proceed both in S_0 and S_1 are displayed in Figure 3.2. For the HBQ normal form in the S_0 state, the calculated

stretching vibrational mode of O–H group is located at 3177 cm^{-1}, whereas it changes to be around 2965 cm^{-1} in S_1 state (with 201 cm^{-1} redshift). Similarly, the O−H stretching bands of HBID, IPDO, IPRO, PDP, and PRP exhibit the redshift of 206, 188, 85, 281, and 392, respectively (see Figure 3.2). These results can indicate that the intramolecular hydrogen bonds were strengthened in the first excited-state.

By comparison of the redshift between HBQ and HBID, it was found that the HBQ has larger red-shifted than HBID, as HBQ has a shorter distance between proton donor and proton acceptor (O···N) than HBID. Likewise, the redshift of IPDO compared with that of IPRO, the redshift of IPDO have larger than IPRO because IPDO has a shorter of O···N distance than IPRO, as well as the redshift of PRP is larger than PDP (the O···N distance of PRP is shorter than PDP). From Figure 3.2, the redshift of PRP is the largest because it has the shortest O···N distance (value listed in Table 3.2). The redshift indicated that the O−H bond strengthened in S_1 state (shortened in S_1 state observed in all compounds). The large redshift suggest that the PT may occur easily in S_1 state. In contrast, the smallest redshift may provide the high PT barrier of ESIPT. Therefore, the stronger of strengthened intramolecular hydrogen bonds might lead to the occurrence of ESIPT.

Table 3.2 Relative O1–H stretching between the S_0 and S_1 states of all compounds

Bond	**State**	**Wavenumber (cm^{-1})**					
		HBQ	**HBID**	**IPDO**	**IPRO**	**PDP**	**PRP**
O–H	S_0	3177	3480	3541	3723	3130	3352
	S_1	2965	3274	3353	3638	2849	2960
Δυ		212	206	188	85	281	392

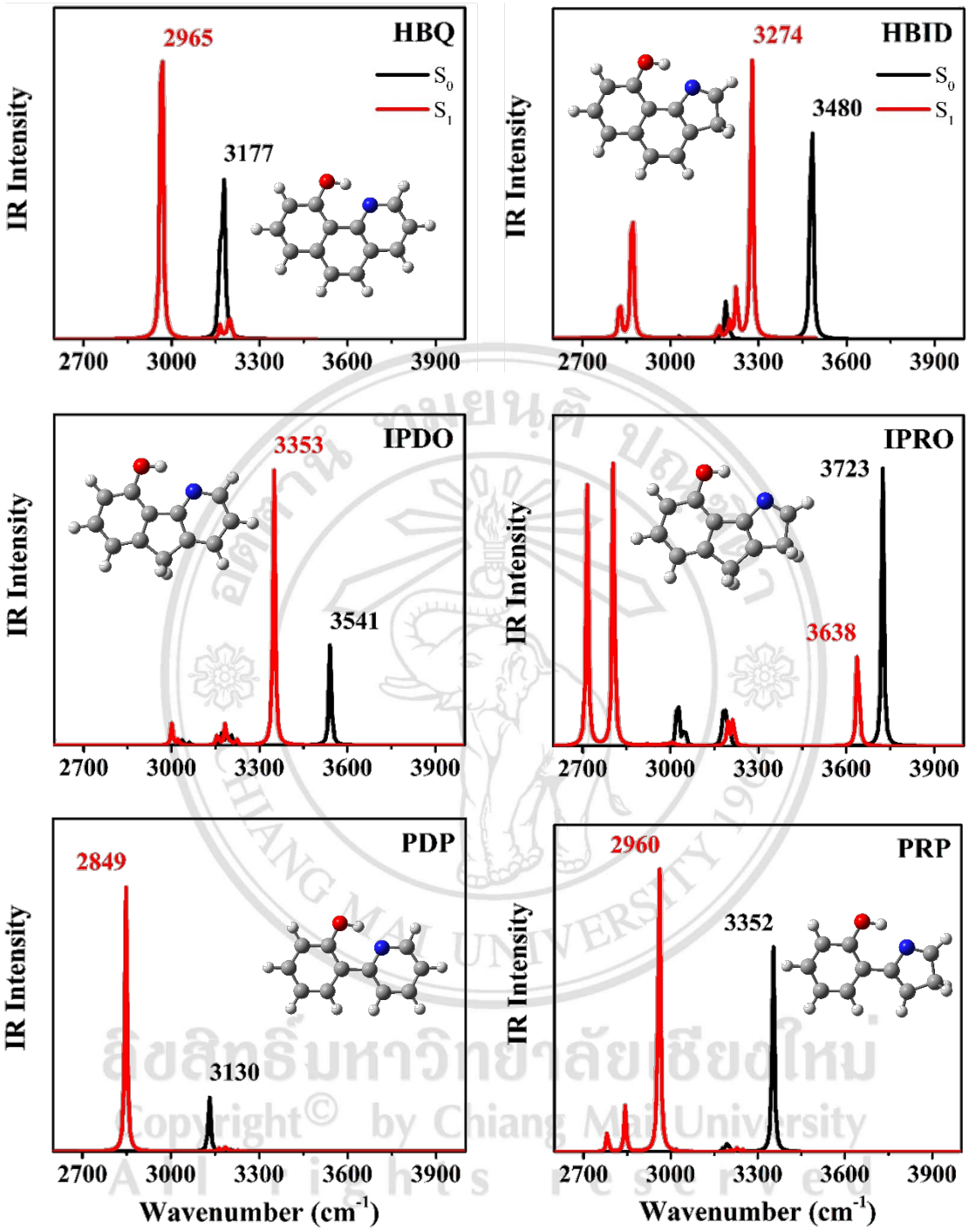

Figure 3.2 The vibrational frequencies of the O–H stretching vibrational mode of the calculated IR spectra of HBQ both in the ground (black line) and the excited-states (red line) of HBQ and its derivative

3.1.2 Electronic spectra and frontier molecular orbitals (MOs)

Absorption (solid black line) and emission (dashed red line) spectra of HBQ and its derivatives based on TD-B3LYP/TZVP level are illustrated in Figure 3.3. In the absorption peak of HBQ is found at 364 nm and its emission peak is observed at 621 nm with the Stokes shift of 257 nm. Our calculated results agreed well with experimental result of absorption peak at 370 nm and emission peak at 609 nm [46]. For HBID, the calculated absorption maxima is 384 nm and its emission peak is 448 nm. The small Stokes shift of 64 nm was observed for HBID. Besides, IPDO, the calculated are show at 305 and 456 nm, Stokes shift is 151 nm. The calculated absorption and emission spectra of IPRO are around 343 and 666 nm. The large Stokes shift is about 323 nm of IPRO. For PDP and PRP, the absorption peaks found at 325 and 359 nm, respectively, and the emission peaks found at 459 and 651 nm, respectively (Stokes shift around 134 for PDP and 292 for PRP).

The Stokes shift of HBQ is larger than that of HBID. The large Stokes shifts originate from the HBQ has six-membered ring in this molecule, but the HBID has five-membered ring. On the other hand, IPRO is larger Stokes shift than IPDO because IPRO has five-membered ring, but the IPDO has six-membered ring, meanwhile, PRP (having five-membered ring) is larger Stokes shifted than IPRO (having six-membered ring). Thus, the geometry change will lead to a small or large shift of the electronic spectra of compounds compared to that of HBQ.

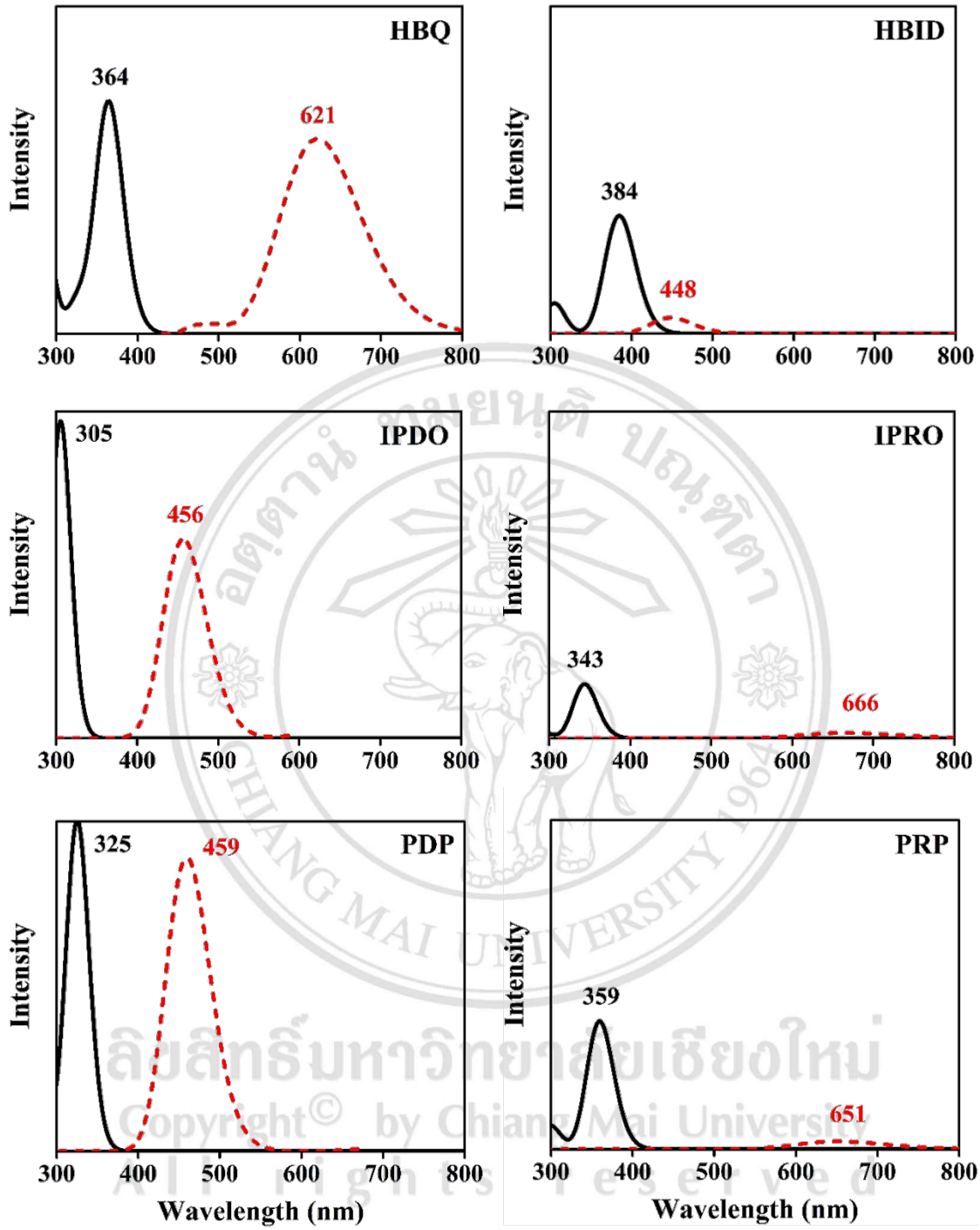

Figure 3.3 Simulated absorption (black solid line) and emission spectra (red dashed line) of HBQ and its derivatives computed at B3LYP/TZVP level

Figure 3.4 shows calculated results of the highest occupied molecular orbital (HOMO) and lowest unoccupied molecular orbital (LUMO) energy levels as well as energy gap (HOMO-LUMO) of normal absorption and tautomer emission of HBQ and its derivatives. For absorption of normal form, energy differences between HOMO of HBQ and its derivatives as well as LUMO are compared. The energy gaps of HBQ, HBID, IPDO, IPRO, PDP, and PRP are 3.88, 3.73, 4.57, 4.16, 4.31, and 3.99 eV, respectively. The energy gaps were found to be in this order: IPDO > PDP > IPRO > PRP > HBQ > HBID. In the case of HBQ compared with HBID, the energy gap of HBQ is higher than that of HBID because the HBQ having pyridine (six-membered ring) ring but HBID having a pyrrole (five-membered ring) ring. The energy gap of IPDO is higher than that of IPRO because of the difference of geometries, IPDO having pyridine ring but IPRO having pyrrole ring as well as PDP is higher of energy gap than that of PRP. From the results, the energy gaps of the compounds have pyridine ring are higher than compounds have pyrrole ring. Theses indicated that the different geometries effect plays an important role in the variations of energy level. For emission of tautomer form, in the compounds have pyrrole ring raise the HOMO energy level and lower LUMO energy level compared to the compounds have pyridine ring. The energy gap of HBQ is 2.67 eV. Changing pyridine to pyrrole ring as HBID (1.54 eV), the red-shifted emission is found when compared to HBQ. The energy gap of IPDO (3.01 eV) is higher than that of IPRO (1.06 eV) by reason of the difference of geometries, IPDO having pyridine ring but IPRO having pyrrole ring. Meanwhile, the PDP is higher of energy gap than that of PRP. From the results, the energy gaps of the compounds have pyridine ring are higher than compounds have pyrrole ring, theses indicated that the pyrrole ring to reduce delocalize of electron which cause low intensity on the ESIPT fluorescence.

The detailed of frontier molecular orbitals (MOs) is very useful to the description of charge transfer change and charge distribution after PT reaction. The MOs (normal form) of the HBQ, HBID, IPDO, IPRO, PDP, and PRP are showed in Figure 3.5. The π character of the HOMO and π* character of the LUMO can be seen clearly. The S_1 of HBQ is a dominant π→π* type from HOMO to the LUMO. From HOMO orbital, electron density completely occupies the whole molecule except on the N atom, while electron density of the LUMO is also delocalized on the whole molecule except on the O–H group (see Figure 3.5). For the other compounds, the frontier MOs give the similar result to

those of HBQ. Moreover, the decrease of electron distribution on the O–H group is expected to directly influence the intramolecular hydrogen bonding.

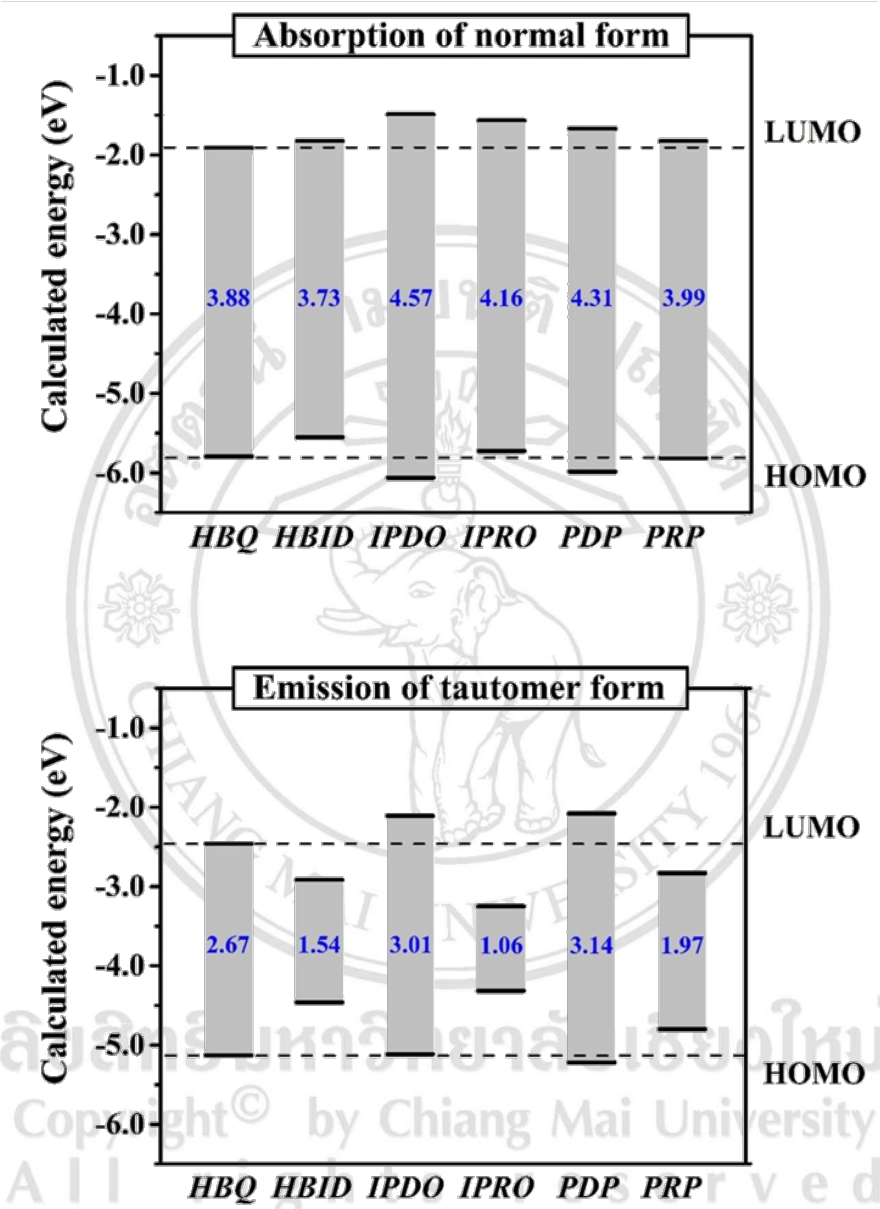

Figure 3.4 Diagram of calculated HOMO and LUMO energy levels as well as HOMO-LUMO gaps (eV) at B3LYP/TZVP level of normal absorption and of tautomer emission of HBQ and its derivatives

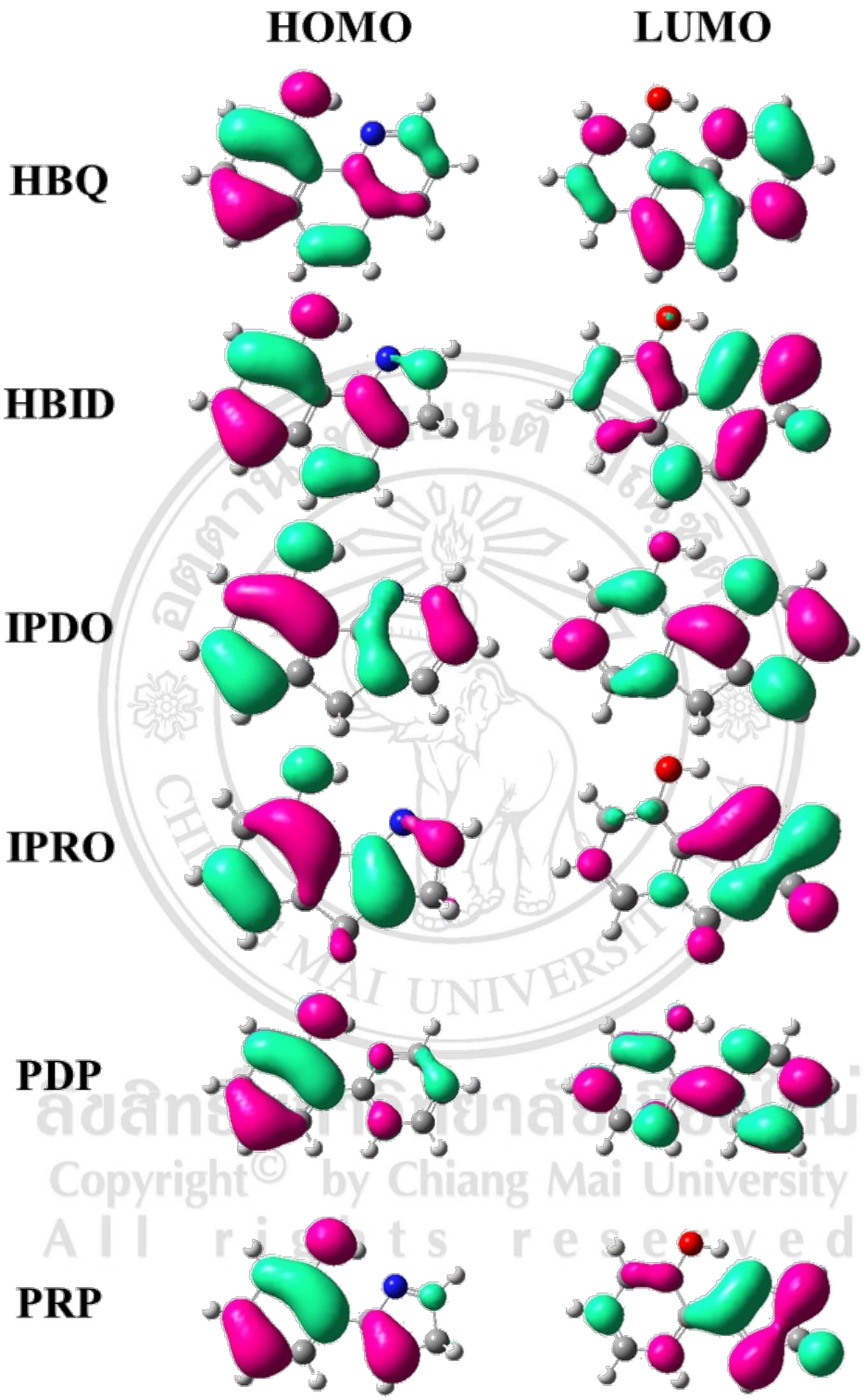

Figure 3.4 Frontier molecular orbitals of normal forms for HBQ and its derivatives computed at B3LYP/TZVP level

Table 3.3 Electronic and photophysical properties of HBQ and its derivatives computed at B3LYP/TZVP level. Calculated normal absorption and tautomer emission (nm, eV), oscillator strength (*f*), and major contributions (%)

Compounds	**Absorption**				**Emission**			
	nm	**eV**	***f***	**MOs** (% **contribution**)	**nm**	**eV**	***f***	**MOs** (% **contribution**)
HBQ	364	3.41	0.127	HOMO→LUMO (93%)	621	1.99	0.107	HOMO→LUMO (96%)
HBID	384	3.23	0.065	HOMO→LUMO (98%)	448	2.76	0.009	HOMO→LUMO (90%)
IPDO	305	4.07	0.1700	HOMO→LUMO (92%)	456	2.71	0.110	HOMO→LUMO (95%)
IPRO	343	3.61	0.030	HOMO→LUMO (97%)	666	1.86	0.003	HOMO→LUMO (100%)
PDP	325	3.81	0.174	HOMO→LUMO (94%)	459	2.70	0.160	HOMO→LUMO (97%)
PRP	359	3.45	0.070	HOMO→LUMO (95%)	651	1.90	0.004	HOMO→LUMO (100%)

3.1.3 Potential energy curves of ESIPT reactions

In order to understand the ESIPT process, the ground and first excited-states potential energy curves (PECs) of HBQ and its derivatives were scanned. The scans were based on the constrained optimizations in their corresponding electronic states at fixed O–H bond length in step of 0.05 Å. The PECs can provide qualitative energetic pathway for the ESIPT proceed of HBQ and its derivatives. The PECs of HBQ and its derivatives are shown in Figure 6. It should be noted that the ground-state potential energy curves (GS-PECs) exists high barrier about 13.22, 41.03, 34.71, 69.29, 11.51, and 22.16 kcal/mol for HBQ, HBID, IPDO, IPRO, PDP, and PRP, respectively. However, the excited-state potential energy curves (ES-PECs) exhibit much lower barriers of 0.47, 0.87, 2.34, 21.10, 0.86 kcal/mol, and no barrier for HBQ, HBID, IPDO, IPRO, PDP and PRP, respectively. Therefore, the ESIPT process is likely to happen in the S_1 state.

The PECs of six-membered ring compounds are also difference from five-membered ring compounds. To illustrate, the different geometries of HBQ (six-membered ring) and HBID (five-membered ring), the PT barrier in S_1 state of HBID is higher than that of HBQ because the distances of N···H, O···N, and C1···N of HBID are longer and its O–H is shorter than HBQ, so these results induce a higher barrier of ESIPT. Similarly, the PT barrier of IPRO (five-membered ring) higher than IPDO (six-membered ring) in S_1 state as the distances of N···H, O···N, and C1···N of HBID are longer and its O–H is shorter than IPDO. Nevertheless, the PT barrier of PDP (six-membered ring) is higher than PRP (five-membered ring), so PT barriers of all compounds are independent on geometry change but they depend on the distances of N···H, O···N, and C1···N.

Furthermore, for PDP and PRP, which in these structures do not have five or six-membered ring in the center of molecule, so the distances between N···H, O···N, and C1···N are found to be the shorter than other compounds and these results leading to the lower PT barrier (0.86 kcal/mol and no barrier for PDP and PRP, respectively). Therefore, the above analysis results have the long distance between O···N correlate with a higher barrier to ESIPT processes, this results agree with previous study [70]. After PT in S_1 state, the skeleton of all compounds are changed confirmed by dynamics simulations.

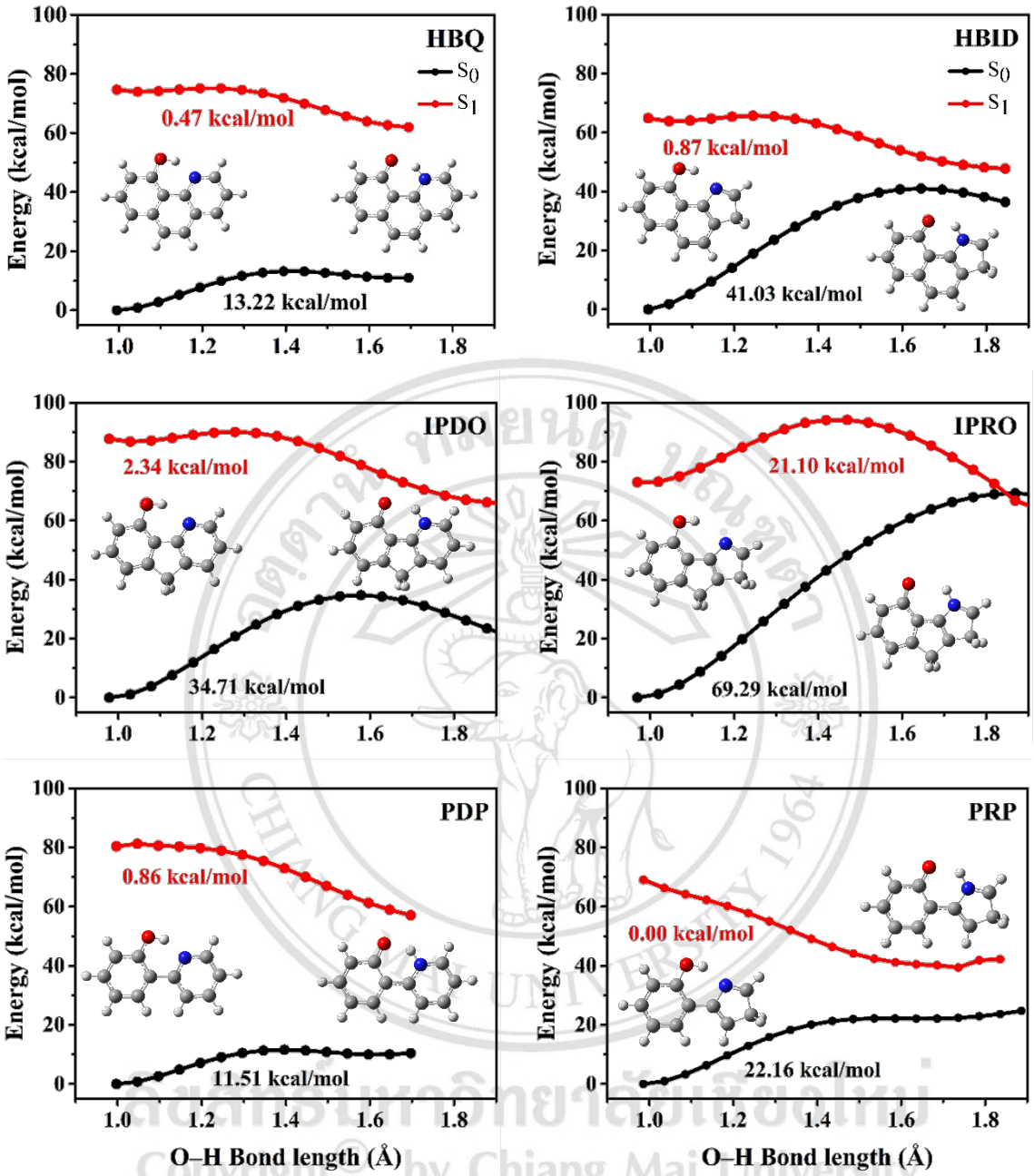

Figure 3.6 The calculated potential energy curves in the S_0 and S_1 states of HBQ and its derivatives. The energies of the S_1 state were calculated using the geometries of the corresponding the S_0 state

3.2 Dynamics simulation

The stimulated trajectories for each compound were classified into two types: (1) ESIPT when the PT processes occurs completely within given simulation time and (2) No transfer when the PT dose not occurs after 300 fs of the simulation time. The numbers of trajectories for each type of reaction, the probability of PT, average time of PT, and PT barrier are summarized in Table 3.3. The results are discussed in the next sections.

Table 3.4 Summary of the excited-state dynamic simulations performed at TD-B3LYP/TZVP and the relative PT barriers (kcal/mol) of all compounds along the ES-PECs

Compound	Reaction		Probability (%)	Time (fs)	PT barrier* (kcal/mol)
	ESIPT	No ESIPT			
HBQ	25	-	100	15 (13-19)	0.47
HBID	24	1	96	43 (40-47)	0.87
IPDO	24	1	96	60 (58-63)	2.34
IPRO	5	20	20	70 (69-78)	21.10
PDP	25	-	100	8 (7-9)	0.86
PRP	25	-	100	22 (19-22)	0.00

* Values are calculated from ES-PECs

3.2.1 10-Hydroxybenzo[*h*]quinoline (HBQ)

This scheme is used to describe the character of the proton transfer dynamics plotted in Fig. 3.7. The average value of breaking (O–H) and forming (N···H) bonds are shown in Figure 3.7a. The intersection between these two bonds indicates PT time constant at 15 fs. This result agree with previous study, Schriever *et al*. reported the ultrafast time scale on proton transfer of 30 fs for classical dynamic simulations [47]. The shaded area in Figure 3.7a is standard deviations of average bonds referring to the time range of proton being transferred from 13-19 fs. The relative energy difference between S_1 and S_0 states (S_1-S_0) shown in Figure 3.7b. The S_1-S_0 energy displayed that the value of energy slightly

decreases in the first 50 fs, after that it is still around 2 eV. This result show that there is no crossing between the S_1 and S_0 states. The average value of torsion angle of C1C2C3N Figure 3.7c is unimportantly different, indicates that no twisting structure of HBQ. More details of PT process are displayed by snapshots of excited state dynamic simulations of HBQ at different time Figure 3.8, in which a normal (N) form start at 0 fs. The H atom departs from phenol to pyridic N atom at 15 fs then after 19 fs the tautomer is formed.

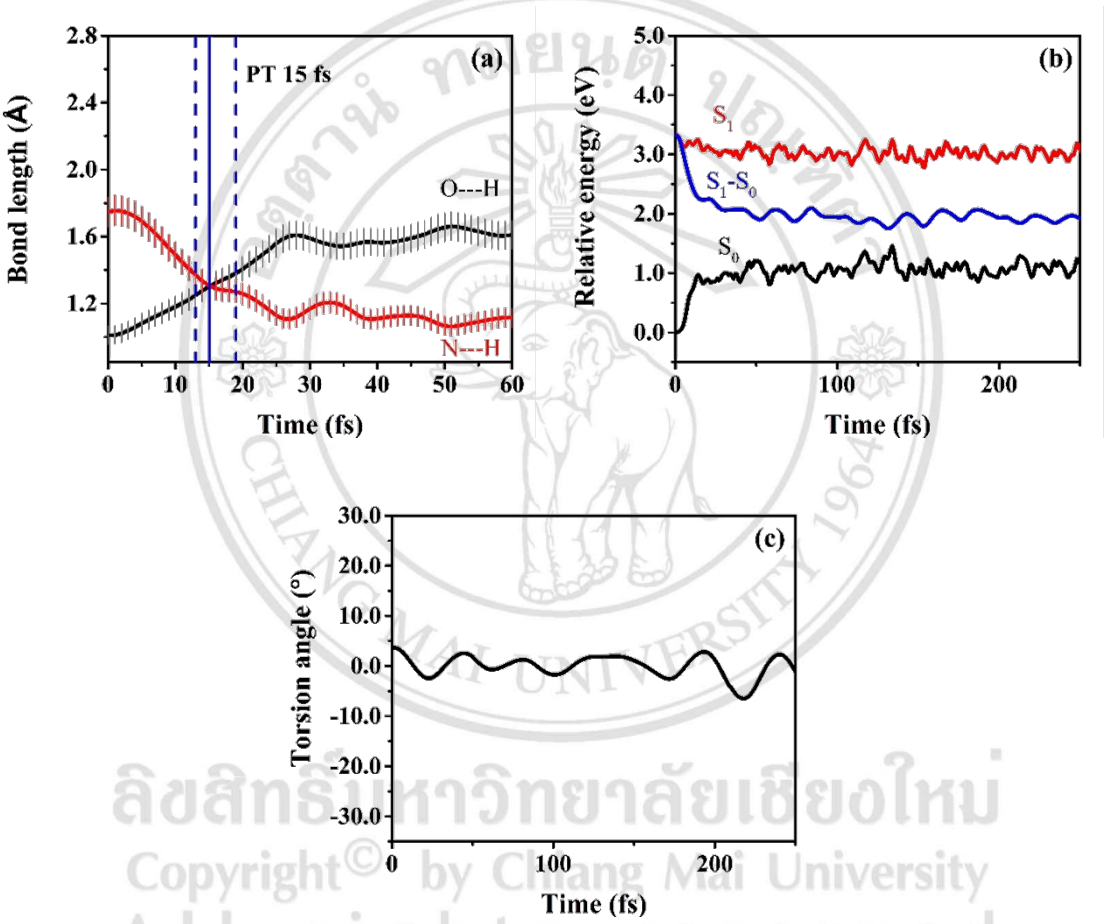

Figure 3.7 Average values for all ESIPT trajectories of the HBQ: (a) Average breaking and forming bonds showing time evolutions, (b) Average relative energies of excited-state (S_1), ground state (S_0), and energy difference of S_1 and S_0 states (S_1-S_0), and (c) Average torsion angle

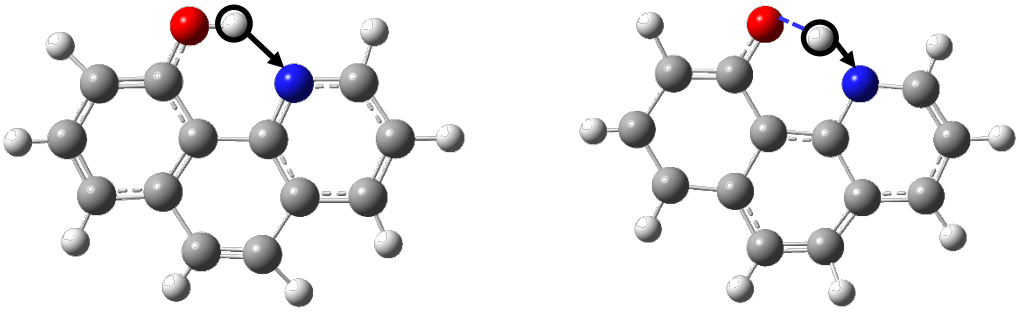

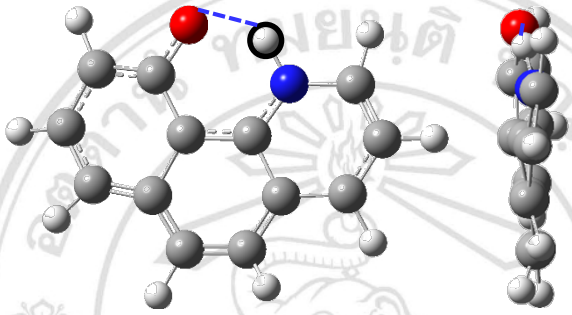

Figure 3.8 Snapshots of the HBQ dynamics showing the time evolutions of the ESIPT reactions through the hydrogen-bonded network. Normal (N), proton transfer (PT), and tautomer (T), the side view of T form shown as the right figure. The values correspond to the average over all ESIPT trajectories in femtosecond

3.2.2 9-Hydroxy-3H-benzo[*g*]indole (HBID)

The ESIPT processes occurred in 24 out of 25 trajectories, while 1 trajectory no ESIPT. Therefore, the PT probability is 96%. The average values for energy and geometric parameter for 24 trajectories following the ESIPT reaction are displayed in Figure 3.9. The average value of breaking (O–H) and forming (N···H) bonds are appeared in Figure 3.9a. The intersection between these two bonds imply PT time constant at 43 fs with in the time range of 40-47 fs, which is about factor two slower than HBQ. The evident pyrrole ring in this compound shows an important role in interacting with the O–H of phenol during the PT proceed, so that PT time take longer compared to that of HBQ. The relative energy difference between S_1 and S_0 presented that the value of energy decreases as the PT proceeds and drops to below 2 eV after 25 fs. This result signify that

there is crossing between the S_1 and S_0 states. The average value of torsion angle of C1C2C3N (Figure 3.9c) is importantly different, indicates that the twisting structure of HBID. The twisting structure of this compound implies that the internal conversion is initiated after ESIPT is finish. Moreover, the details of PT process are shown by snapshots of excited state dynamic simulations of HBID at different time (Figure 3.10), in which a normal (N) form start at 0 fs. The H atom departs from phenol to pyridic N atom at 43 fs then after 47 fs the tautomer is formed.

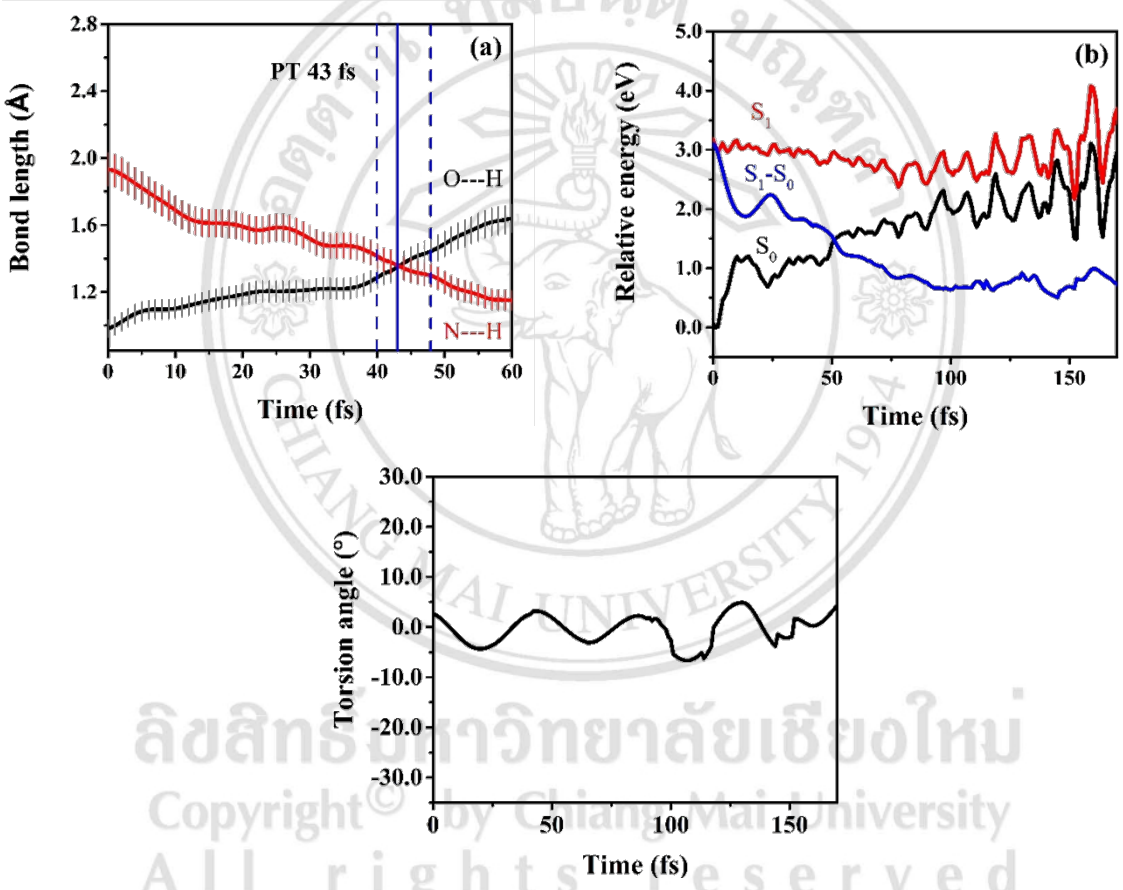

Figure 3.9 Average values for all ESIPT trajectories of the HBID: (a) Average breaking and forming bonds showing time evolutions, (b) Average relative energies of excited-state (S_1), ground state (S_0), and energy difference of S_1 and S_0 states (S_1-S_0), and (c) Average torsion angle

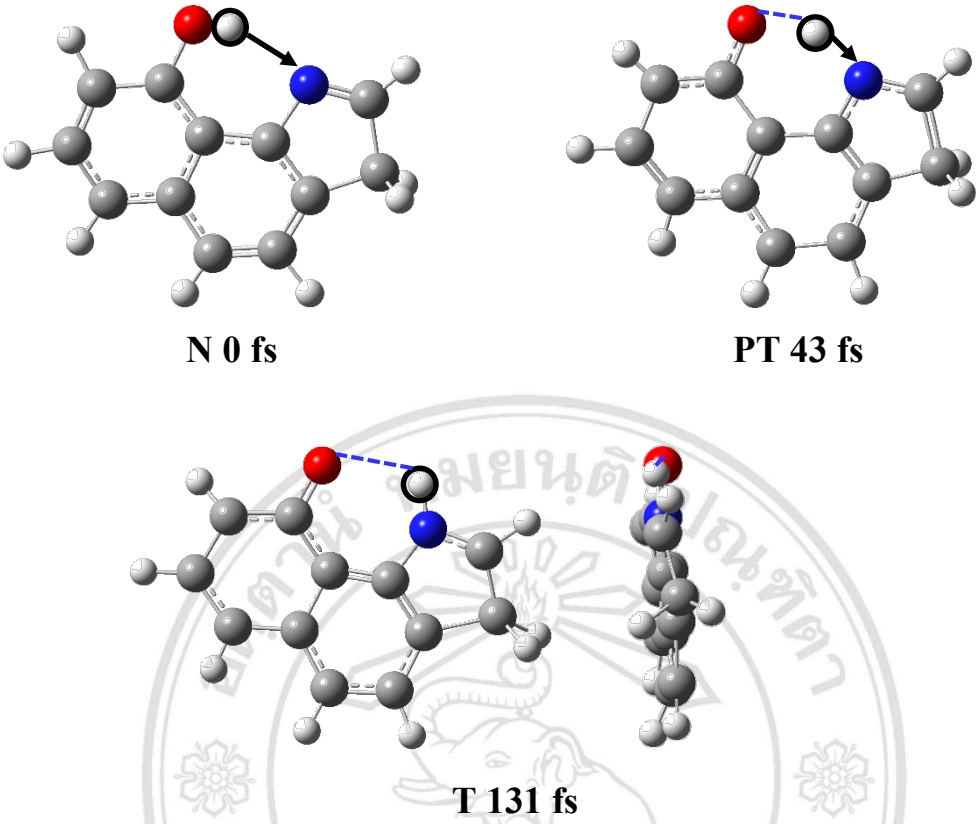

Figure 3.10 Snapshots of the HBID dynamics showing the time evolutions of the ESIPT reactions through the hydrogen-bonded network. Normal (N), proton transfer (PT), and tautomer (T), the side view of T form shown as the right figure. The values correspond to the average over all ESIPT trajectories in femtosecond

3.2.3 5H-indeno[1,2-*b*]pyridine-9-ol (IPDO)

For IPDO, 24 trajectories displayed the ESIPT, while one trajectory displayed no ESIPT within the simulation time. Thus, the PT reaction probability is 96% (Table 3.2). The average values for energy and geometric parameter following the ESIPT processes are demonstrated in Figure 3.11. In Figure 3.11a shows the average value of breaking (O–H) and forming (N···H) bonds. The intersection between the curves suggests that the PT time occurs at 60 fs. The time range of proton being transferred from 58-63 fs. Figure 3.11b displays the relative energy difference between S_1 and S_0 states gradually decrease as the PT proceeds and it is lower than 2 eV indicating that the structure of IPDO is twist. This twisting of IPDO is supported by the average value of torsion angle of C1C2C3N (Figure 3.11c). The details of PT process are illustrated by snapshots of excited state

dynamic simulations of IPDO at different time (Figure 3.12), in which a normal (N) form start at 0 fs. The H atom departs from phenol to pyridic N atom at 60 fs then after 63 fs the tautomer is formed.

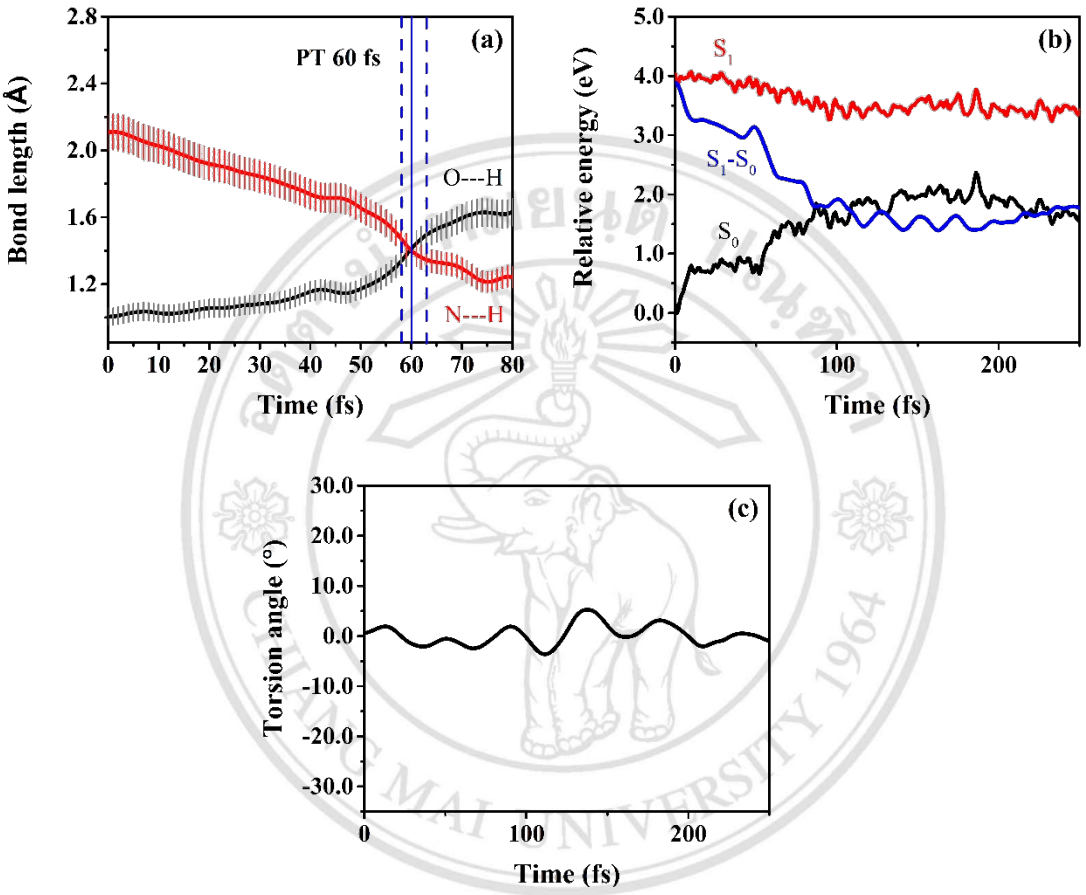

Figure 3.11 Average values for all ESIPT trajectories of the IPDO: (a) Average breaking and forming bonds showing time evolutions, (b) Average relative energies of excited-state (S_1), ground state (S_0), and energy difference of S_1 and S_0 states (S_1-S_0), and (c) Average torsion angle

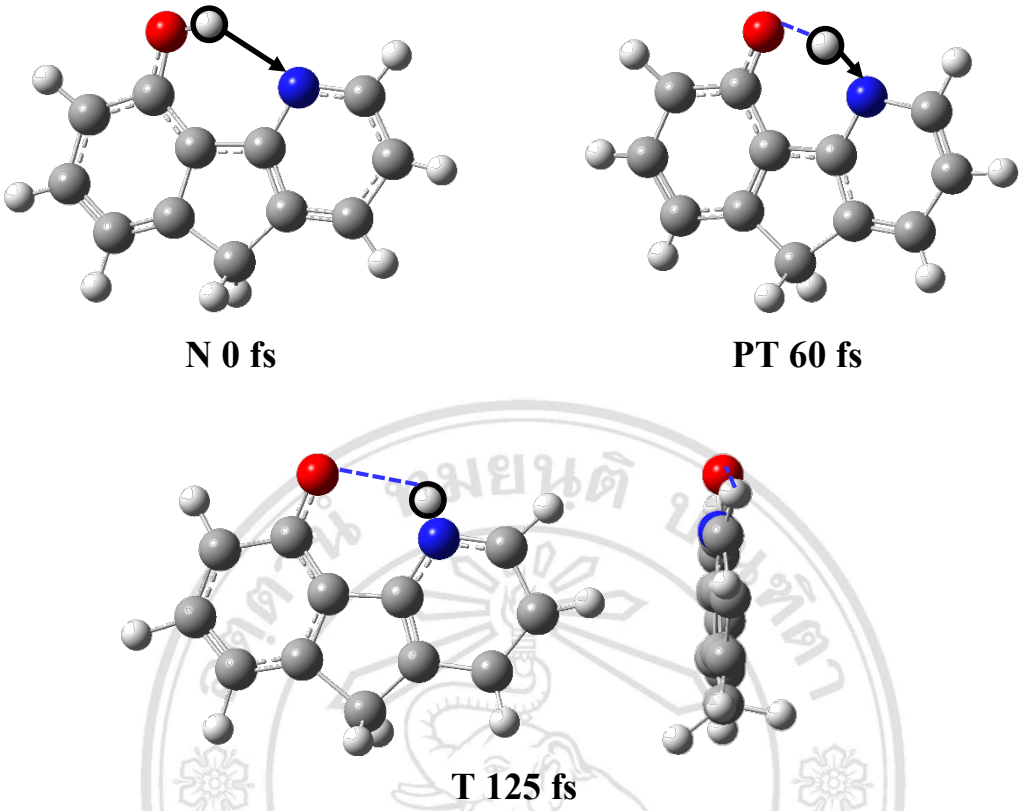

Figure 3.12 Snapshots of the IPDO dynamics showing the time evolutions of the ESIPT reactions through the hydrogen-bonded network. Normal (N), proton transfer (PT), and tautomer (T), the side view of T form shown as the right figure. The values correspond to the average over all ESIPT trajectories in femtosecond

3.2.4 3,4-dihydroindene[1,2-*b*]pyrrole-8-ol (IPRO)

For IPRO, five trajectories exhibited the ESIPT and 20 trajectories exhibited no ESIPT reaction within 300 fs. Therefore, the PT reaction probability is 20% (Table 3.2). The average values for energy and geometric parameter for five trajectories following the ESIPT reaction are seen in Figure 3.13. The evolution of the average values of breaking bond (O–H) and forming bond (N···H) is plotted in Figure 3.13a. The PT process for IPRO occurred at 70 fs within the time range of 69-78 fs. The relative energy of S_1-S_0 gradually decrease as the PT proceeds and drops to below 2 eV (Figure 3.13b) due to slightly non-planar conformation of IPRO. This implies that the internal conversion is initiated after ESIPT is complete. The average value of torsion angle of C1C2C3N shown in Figure 3.13c reveals that skeleton of IPRO is more twisted after the ESIPT at around

70 fs. The snapshots of average trajectories long the PT process are shown in Figure 3.14, in which a normal (N) form start at 0 fs, PT. The H atom departs from phenol to pyridic N atom at 70 fs then after 78 fs the tautomer is formed.

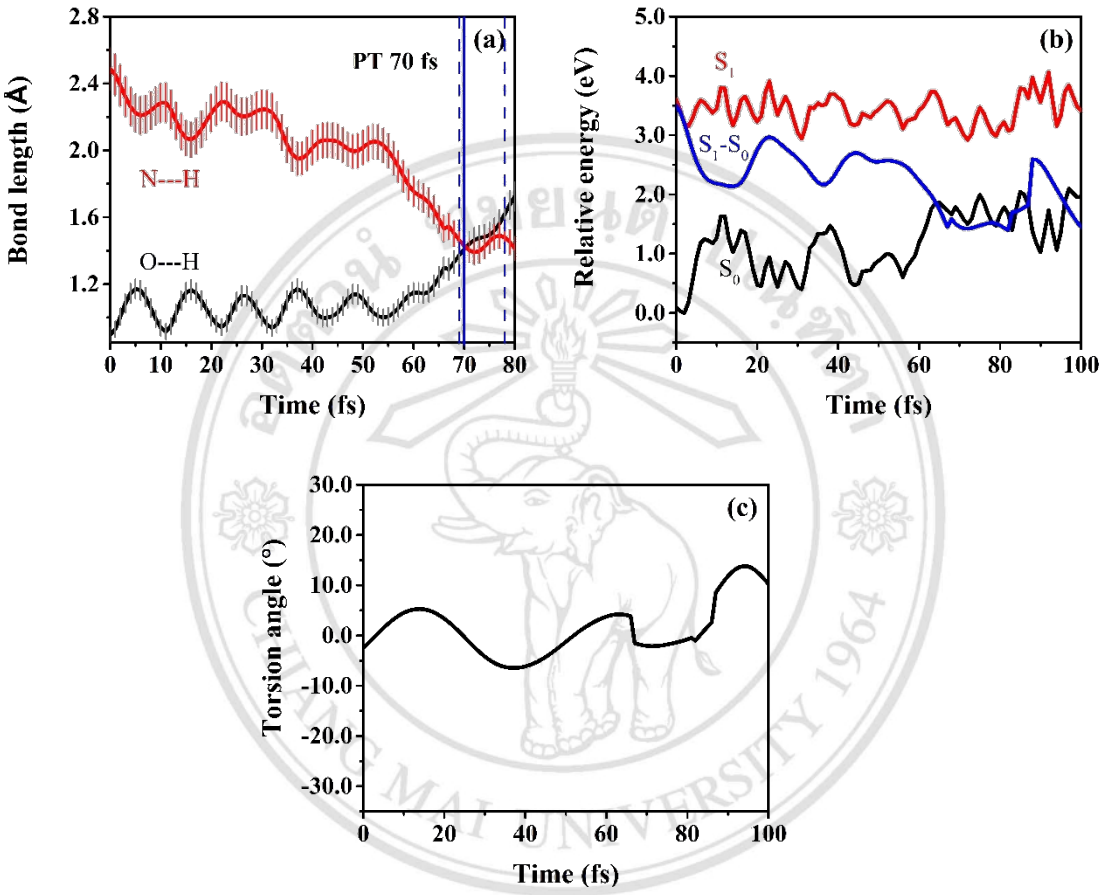

Figure 3.13 Average values for all ESIPT trajectories of the IPRO: (a) Average breaking and forming bonds showing time evolutions, (b) Average relative energies of excited-state (S_1), ground state (S_0), and energy difference of S_1 and S_0 states (S_1-S_0), and (c) Average torsion angle

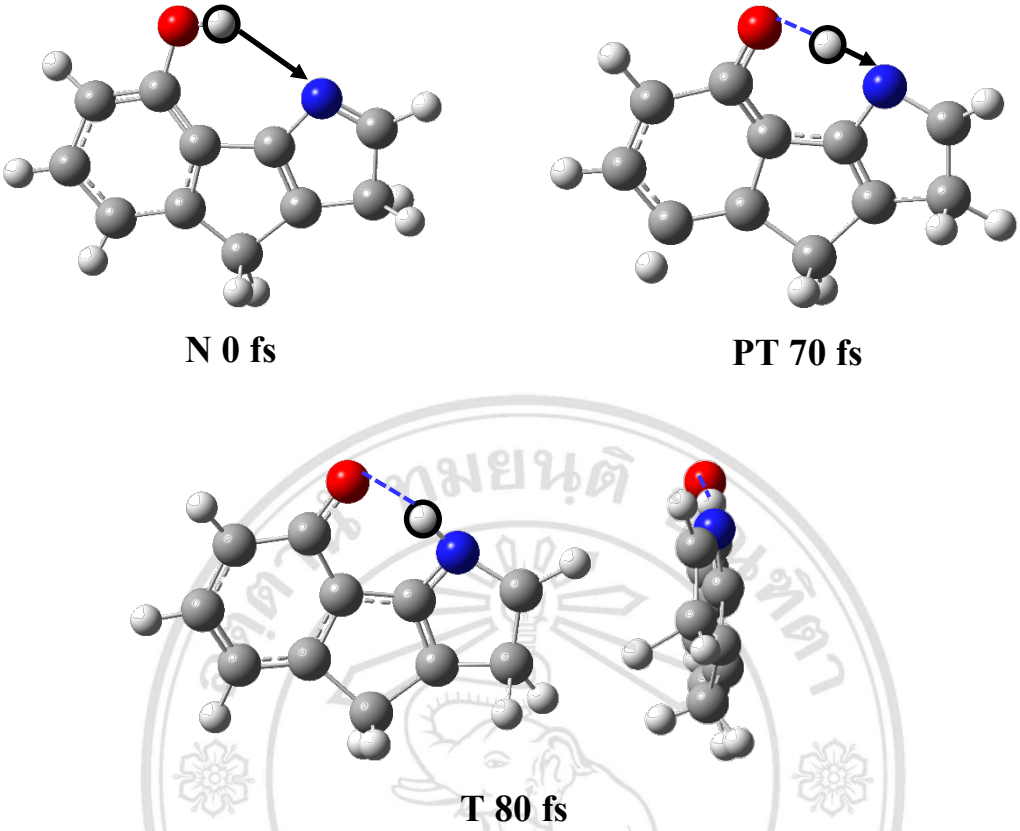

Figure 3.14 Snapshots of the IPRO dynamics showing the time evolutions of the ESIPT reactions through the hydrogen-bonded network. Normal (N), proton transfer (PT), and tautomer (T), the side view of T form shown as the right figure. The values correspond to the average over all ESIPT trajectories in femtosecond

3.2.5 2-Pyridin-2-yl)phenol (PDP)

The ESIPT reaction occurred in 25 trajectories, so the PT probability is 100% (Table 3.2). Average values for energy and geometric parameter for all trajectories following the ESIPT reaction are shown in Figure 3.15. The evolution of the average values of breaking bond (O–H) and forming bond (N···H) is plotted in Figure 3.15a. The PT process for PDP occurred at 8 fs within the time range of 7-9 fs. The relative energy difference of S_1-S_0 drops to below 2 eV (in Figure 3.15b) at about 10 fs right after PT due to gradual twist of C1C2C3N from planarity. This suggests that internal conversion is quickly initiated after ESIPT is achieved, supported by torsion angle changes of both front and back C1C2C3N as shown in Figure 3.15c. In Figure 3.15c, the C1C2C3N torsion changes was divided into two type; (a) front (red line) and (b) back (black line) out-of-

plane C1C2C3N. Snapshots of average trajectories (Figure 3.16) illustrate the ESIPT reaction as the proton moves along the intramolecular hydrogen bond. The snapshots of average trajectories long the PT process are shown in Figure 3.16, in which a normal (N) form start at 0 fs, PT. The H atom departs from phenol to pyridic N atom at 8 fs then after 9 fs the tautomer is formed.

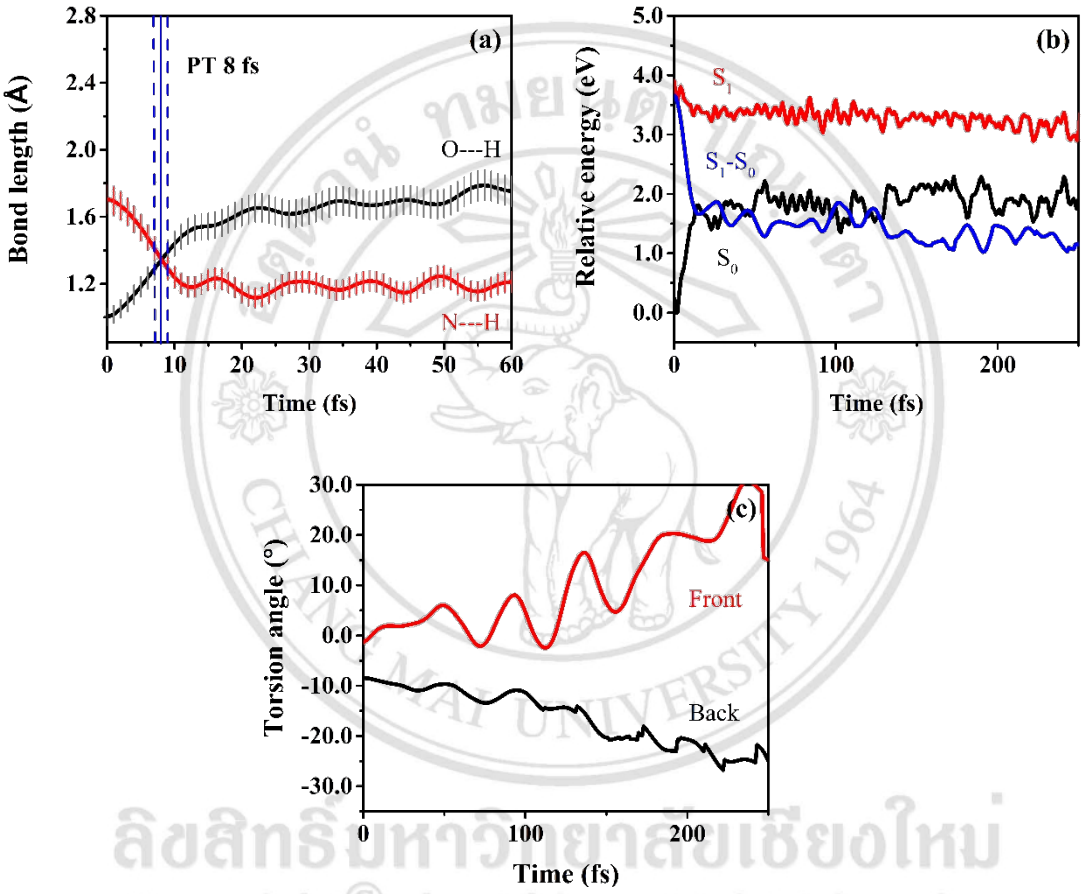

Figure 3.15 Average values for all ESIPT trajectories of the PDP: (a) Average breaking and forming bonds showing time evolutions, (b) Average relative energies of excited-state (S_1), ground state (S_0), and energy difference of S_1 and S_0 states (S_1-S_0), and (c) Average torsion angle

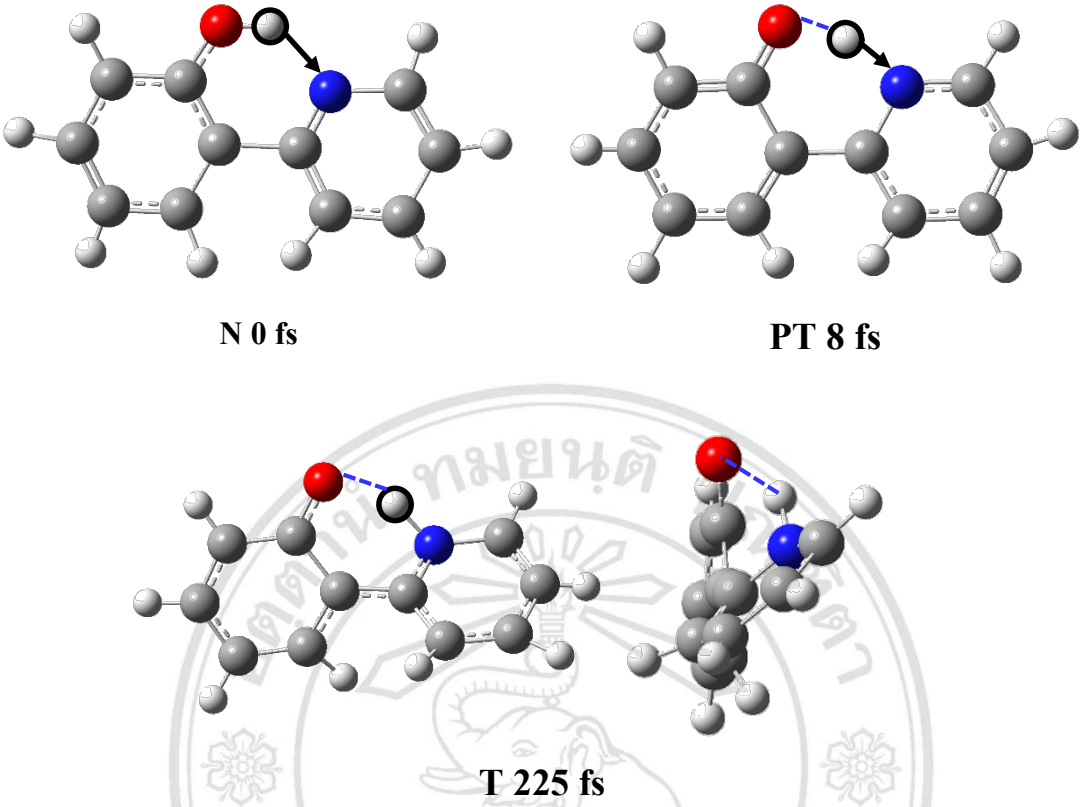

Figure 3.16 Snapshots of the PDP dynamics showing the time evolutions of the ESIPT reactions through the hydrogen-bonded network. Normal (N), proton transfer (PT), and tautomer (T), the side view of T form shown as the right figure. The values correspond to the average over all ESIPT trajectories in femtosecond

3.2.6 2-(4H-pyrrol-2-yl)phenol (PRP)

From 25 trajectories, all trajectories show ESIPT completely. Thus, the reaction probability is 100%. Average values for energy and geometric parameter for all trajectories following the ESIPT reaction are shown in Figure 3.17. The evolution of the average values of breaking bond (O–H) and forming bond (N···H) is shown in Figure 3.17a. The intersection between two lines indicates that the PT occurs at 22 fs. Figure 3.17b displayed that the average energy difference between S_1 and S_0 states decreases to below 2 eV, this suggesting that the structure of PRP occur internal conversion is quickly initiated after ESIPT is completed. The twisted of PRP is confirmed by torsion angle changes of both front and back C1C2C3N as illustrated in Figure 3.17c. In Figure 3.17c, the C1C2C3N torsion changes was divided into two type; (a) front (red line) and (b) back

(black line) out-of-plane C1C2C3N. The snapshots of average trajectories long the PT process are shown in Figure 3.18, in which a normal (N) form start at 0 fs, PT. The H atom departs from phenol to pyridic N atom at 22 fs then after 22 fs the tautomer is formed.

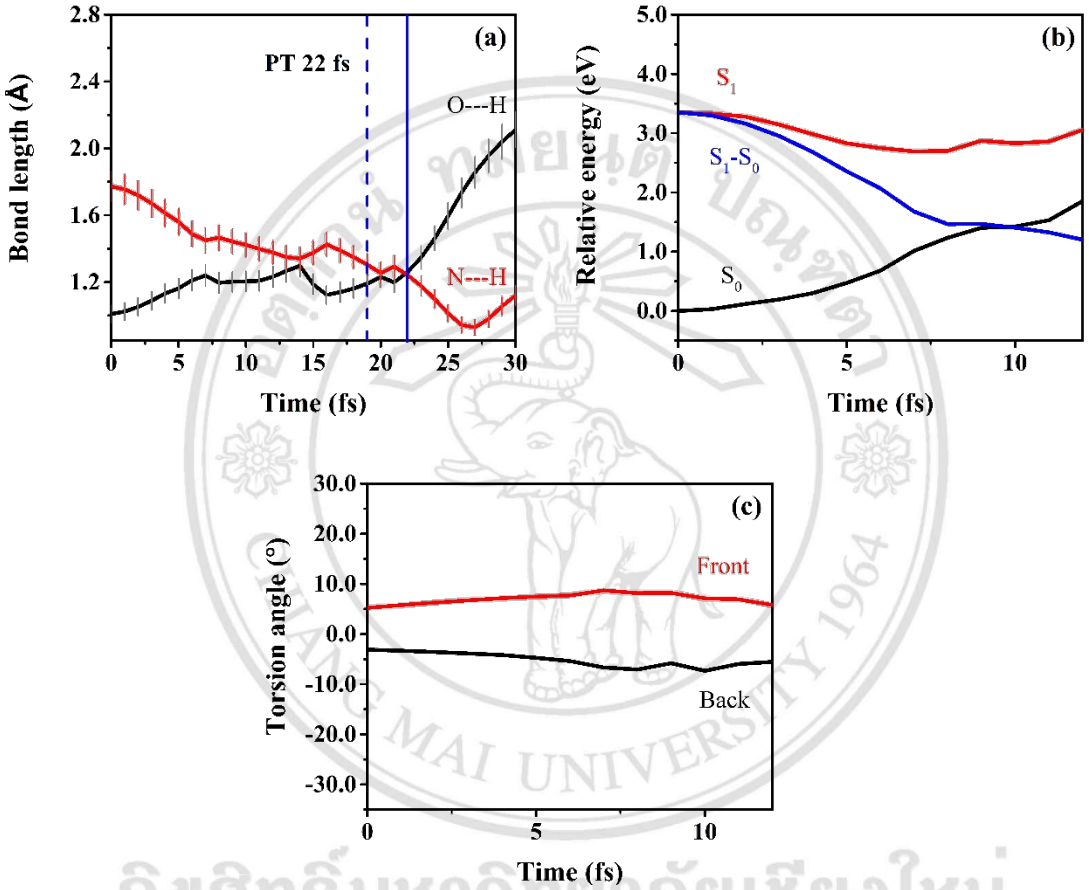

Figure 3.17 Average values for all ESIPT trajectories of the PRP: (a) Average breaking and forming bonds showing time evolutions, (b) Average relative energies of excited-state (S_1), ground state (S_0), and energy difference of S_1 and S_0 states (S_1-S_0), and (c) Average torsion angle

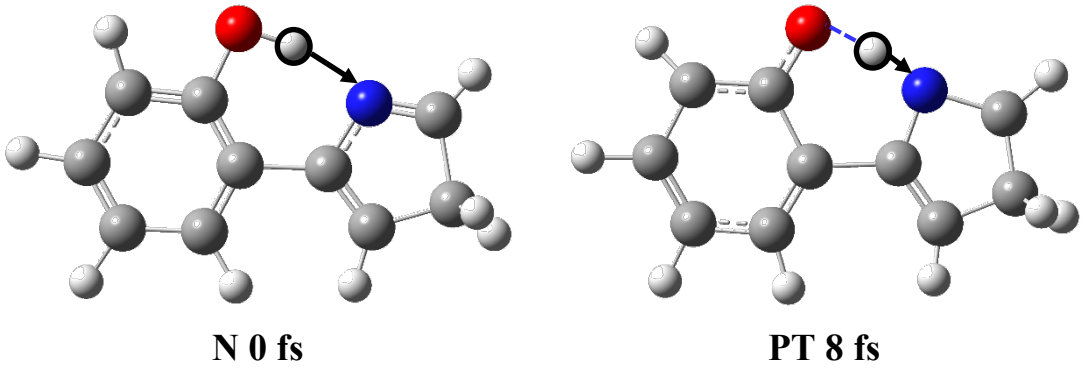

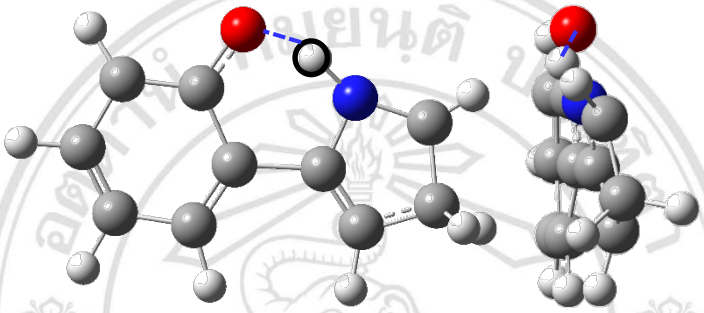

Figure 3.18 Snapshots of the PRP dynamics showing the time evolutions of the ESIPT reactions through the hydrogen-bonded network. Normal (N), proton transfer (PT), and tautomer (T), the side view of T form shown as the right figure. The values correspond to the average over all ESIPT trajectories in femtosecond

3.3 Comparative analysis

The PT barriers are anti-correlate with probabilities of ESIPT. The ESIPT probabilities of HBQ, HBID, IPDO, IPRO, PDP, and PRP are 100%, 96%, 96%, 20%, 100%, and 100%, respectively (Table 3.3). It is worth noting that the structural change plays an important role in reducing the PT barrier of ESIPT reaction and the PT times.

Comparison between HBQ and HBID, the PT barrier of HBQ is lower than HBID but the ESIPT probabilities of HBQ is higher than HBID. The geometries of both structures are difference; the HBQ has pyridine ring near six-membered ring but HBID has a pyrrole ring. The different geometries lead to the N···H, O···N, and C1···N distances, the PT barriers, and PT times are change. In this case, HBID has the distances of N···H,

O···N, and C1···N are longer than HBQ, the long distance between proton donor-acceptor is the cause of the long PT time and the high PT barrier. Moreover, the long distance between proton donor-acceptor causes of low probability of ESIPT, so the ESIPT probabilities of HBID is lower than HBQ (see Table 3.3).

For IPDO compared with IPRO, the PT barrier of IPDO is lower than IPRO but the ESIPT probabilities of IPDO (96%) is higher than IPRO (20%). The geometries of both structures are difference; the IPDO has pyridine ring near five-membered ring but IPRO has a pyrrole ring. The different geometries lead to the N···H, O···N, and C1···N distances, the PT barriers, and PT times are change. The IPRO has the distances of N···H, O···N, and C1···N are longer than IPDO, the long distance between proton donor-acceptor is induce the long PT time and the high PT barrier. Moreover, the long distance between proton donor-acceptor causes of low probability of ESIPT (see Table 3.3).

Comparison between PDP and PRP, the geometries of PDP and PRP are different from other compounds (HBQ, HBID, IPDO, and IPRO). The both compounds do not have five or six membered ring in the middle molecules. The PT times of PDP and PRP are high probability of ESIPT (100%), the ESIPT of probabilities of both compounds occur in ultrafast timescale less than 25 fs, and PT barriers are lower than 1 kcal/mol (0.86 kcal/mol of PDP and 0.00 kcal/mol of PRP). The PT barrier of PRP is lower than PDP because the O···N distance in PRP is shorter than PDP, this result is responsible for the low barrier for PT between O and N atoms. On the other hand, the PT time of PRP is slower than PDP after PT are complete, the twisted skeleton behavior is found in both systems (see snapshots T form in Figure8c for PDP and Figure S3c for PRP). It means, from Table 3.1 point of view that the distances of N···H and C1···N in the PDP are shorter than PRP, induce the faster PT time in PDP.

Comparison between HBQ and IPDO, the PT barrier of HBQ is lower than IPDO. The geometries of both structures are difference; the HBQ has six-membered ring in the middle structure but IPDO has a six-membered ring. The different geometries lead to the N···H, O···N, and C1···N distances, the PT barriers, and PT times are change. In this case, IPDO has the distances of N···H, O···N, and C1···N are longer than HBQ, the long distance between proton donor-acceptor is the cause of the long PT time and the high PT barrier.

Moreover, the long distance between proton donor-acceptor causes of low probability of ESIPT, so the ESIPT probabilities of IPDO is lower than HBQ (see Table 3.3).

Comparison between HBQ and PDP, the geometry of PDP is different from HBQ. The PDP do not have five or six membered ring in the middle structure. The PT times of HBQ and PDP are high probability of ESIPT (100%), the PT times of HBQ is 15 fs and PDP is 8 fs. The HBQ has the distances of N···H, O···N, and C1···N are longer than PDP, the long distance between proton donor-acceptor is the cause of the long PT time. The PT barrier of HBQ (0.47 kcal/mol) is lower than PDP (0.86 kcal/mol), this result is revered above discussions because the twisted skeleton behavior is found in PDP after PT processes (see snapshots T form in Figure 3.16).

Comparison between HBID and IPRO, the PT barrier of HBID is lower than IPRO but the ESIPT probabilities of HBID (96%) is higher than IPRO (20%). The geometries of both structures are difference; the HBID has six-membered ring in the middle structure but IPRO has a six-membered ring. The different geometries lead to the N···H, O···N, and C1···N distances, the PT barriers, and PT times are change. In this case, IPRO has the distances of N···H, O···N, and C1···N are longer than HBID, the long distance between proton donor-acceptor is the cause of the long PT time and the high PT barrier. Moreover, the long distance between proton donor-acceptor causes of low probability of ESIPT (see Table 3.3).

Comparison between HBID and PRP, the geometry of PRP is different from HBID. The PDP do not have five or six membered ring in the middle structure. The different geometries lead to the N···H, O···N, and C1···N distances, the PT barriers, and PT times are change. The HBID has the distances of N···H, O···N, and C1···N are longer than PRP, the long distance between proton donor-acceptor is the cause of the long PT time and the high PT barrier. Moreover, the long distance between proton donor-acceptor causes of low probability of ESIPT, so the ESIPT probabilities of HBID is lower than PRP (see Table 3.3).

As discusses above, it is worth noting that the interplay of skeletal deformation plays an important role differ in the PT barrier of ESIPT reaction, the PT times and probabilities of ESIPT. The difference in the geometries can be seen, IPRO compared

with PRP, The IPRO has the longest distances of O···N, N···H and C1···N, the highest PT barrier of ESIPT, the slowest PT time, and the lowest of probability of ESIPT. On the other hand, the PRP has the shortest distances of O···N, the lowest PT barrier of ESIPT, and the high probability of ESIPT.